

THE THERMAL PERFORMANCE OF PHASE-CHANGE HEAT STORAGE BUILDING THROUGH COUPLED HEAT TRANSFER METHODS

B. ZHANG*, W.LIU, S. LI, Q. SUN

College of Electromechanical Engineering, Qingdao University of Science and Technology, Qingdao 266061

In this study, expanded graphite (EG) and high-density polyethylene (HDP) were used to formulate a new shape-stabilised phase-change materials (SSPCM) with increased thermal conductivity and stability. A full size two-dimensional heat transfer model was conceptualized from an under-floor electric heating system with SSPCM floor. The influence of various factors (thickness of SSPCM layer, under-floor heating flux and thermal conductivity of SSPCM) on the room thermal performance was analyzed through dynamic simulation. In addition to calculation of heat transfer in the phase change from solid to liquid, various heat transfer mechanisms of the coupled problems were considered in the model. Thermal conductivity evidently influences indoor air temperature; that is, high thermal conductivity leads to improved heat diffusion. Moreover, indoor air temperature does not increase with increasing thickness of the layer. Heat storage duration must be controlled in the case when the floor temperature becomes too high and the SSPCM layer is less than 20 mm thick. Furthermore, high under-floor heating flux results in a high indoor air temperature. Thus, the investment and indoor air comfort should be balanced.

(Received June 19, 2017; Accepted September 13, 2017)

Keywords: Phase-change material, PCM heat storage building, Radiant floor system, Indoor thermal comfort

1. Introduction

Thermal storage can match the supply and demand when these factors do not coincide with time. The energy consumption of a building for heating and cooling can be effectively reduced by incorporating phase-change materials (PCMs) in the walls, windows, ceilings and floors of the building^[1-3].

Shape-stabilised PCM (SSPCM) is a new type of PCM that has gained increasing attention. SSPCM exhibits large apparent specific heat, suitable thermal conductivity and ability to maintain the shape of PCM stabilised in the phase-change process^[4-8]. Xiao et al.^[5] studied the preparation and performance of shape-stabilised PCMs for thermal storage. However, the low thermal conductivity of SSPCM may decrease heat storage capacity and release rates during melting and solidification^[9, 10].

The thermal properties of a room can be analyzed by incorporating latent heat thermal energy storage (LHTES) systems with SSPCM in experiments^[11]; however, these systems feature device complexity, require various operating conditions and employ costly, time consuming and inefficient experiment procedures. With the development of computer technology, numerical simulation has gradually become an important method for obtaining and analyzing data under different operating conditions^[12-15].

The dynamic energy performance of buildings incorporating LHTES systems with SSPCM must be elucidated to allow building researchers and practitioners to understand the building temperature response characteristics and the economic feasibility of PCM.

*Corresponding author: zb-sh@163.com

Currently, researchers perform simulations on building floors incorporated with SSPCM. Xu et al. ^[16] studied a kind of under-floor electric heating system with SSPCM plates and analyzed the effects of various factors on thermal performance. Although many researchers carried simulations using the full size of room with SSPCM, they proposed many simplifications on the calculation; these simplifications include the use of the air domain as one particle, simplified the envelope wall as thermally insulated, set constant temperature or heat flux on the floor surface and considered convection without radiation ^[17–21].

A heat transfer process including convection or radiation is conducted between solid surfaces and air, which makes the heating system complicated. In addition, the indoor temperature is related to climate conditions, air exchange rate, room size, wall thickness and occupation rate and activity, resulting in a fluctuating indoor temperature. In this situation, the lumped parameter method does not allow detailed evaluation of the velocity and temperature in the space, which is increasingly important as the indoor design of buildings are becoming complicated.

In this work, PCMs, which consist of paraffin, high-density polyethylene (HDPE) as matrix and expanded graphite (EG) as heat conduction enhancement agent, were generated through a self-established experimental device. The thermal properties of SSPCMs were tested using differential thermal analysis.

A full-size two-dimensional heat transfer model was abstracted from a kind of under-floor electric heating system with SSPCM floor. By using the model, a dynamic simulation of the influence of various factors (thickness of SSPCM layer, under-floor heating flux and thermal conductivity of SSPCM) on thermal performance of room was analyzed. Aside from the calculation of heat transfer in the phase change from solid to liquid, a variety of heat transfer mechanism of the coupled problems were also considered in this model.

2. Production of SSPCM

The structure of EG is loose and porous wormlike. Moreover, EG has good thermal conductivity, is corrosion resistant and is capable of withstanding high temperatures. To improve the thermal conductivity of SSPCM, EG was chosen as a heat conduction enhancement agent in this study.

To manufacture SSPCM, an experimental platform was built, as shown in Fig. 1. The device mainly consists of five parts: iron stand, electric mixer, mixer stick, three-necked flask and electric heating sleeve.

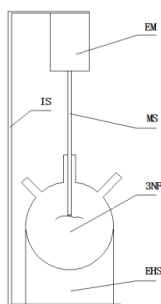


Fig. 1 Experimental platform. Iron stand, IS; electric mixer, EM; mixer stick, MS; three-necked flask, 3NF; electric heating sleeve, EHS.

The materials used in the experiment include paraffin with melting temperature of 28 °C, HDPE and EG. The brief production process of the new SSPCM is as follows. First, maintain the supply of heat, and then stir the paraffin compound and HDPE together until they completely melted. Next, add a moderate amount of EG and continue stirring until completely uniform. Afterward, place the SSPCM in a cooler with a vacuum condition for approximately 24 h. Fig. 2 shows the SSPCMs with different percentages of EG.

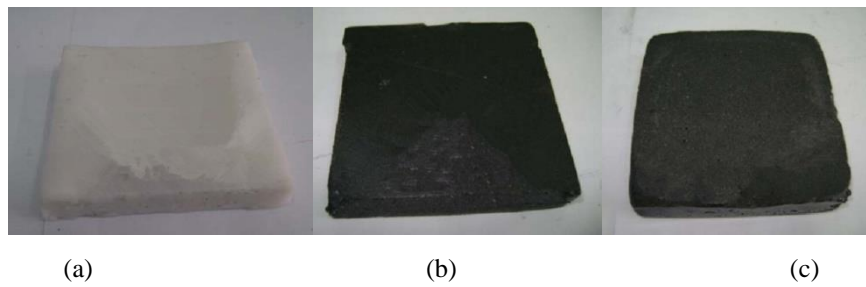


Fig. 2 SSPCMs with different percentages of EG.
(a) 0 wt% EG, (b) 2 wt% EG and (c) 5 wt% EG.

3. Simulation of the SSPCM Room

A typical SSPCM room with internal dimensions of 5 m (depth) \times 4 m (width) \times 3 m (height) was adapted as the calculation model (Fig. 3). The SSPCM room includes two main parts, the one is air domain and the other one is the floor system, which includes a 50 mm-thick polystyrene insulation layer, a 40 mm-thick PCM plate layer, a 20 mm-thick marble layer and an under-floor electric heating layer.

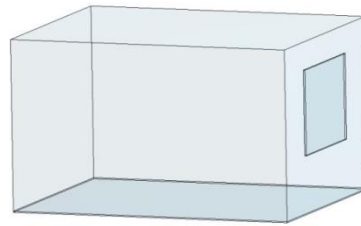


Fig. 3 Selected building for analysis.

Various factors including thickness of SSPCM layer, under-floor heating flux, thermal conductivity and heat fusion of SSPCM are listed in Table 1.

Tab. 1 Thermal physical properties of SSPCM.

λ (W/m·K)	d (mm)	q (W/m ²)	L (kJ/kg)
0.5	20	150	150
1.5	30	200	200
4.5	40	250	250

3.1 Governing equations

The following assumptions were made to simplify the analysis:

- (1) Thermal physical properties of building are constant during melting or freezing process.
- (2) The natural convection during melting and the sub-cooling effect during solidification for PCM are negligible.
- (3) The side surfaces of SSPCM and marble are thermally insulated.

In this study, an enthalpy–porosity technique ^[17–21] was utilized to model such dynamic heat transfer process, and the governing equation is

$$\frac{\partial(\rho h)}{\partial \tau} = \frac{\partial}{\partial x} \frac{\partial(\lambda T)}{\partial x} + \frac{\partial}{\partial y} \frac{\partial(\lambda T)}{\partial y} \quad (1)$$

where h is the enthalpy, T is the temperature, ρ is the density, τ is the time enthalpy. Note that Eq. (1) is in terms of two unknown variables, i.e. the enthalpy and temperature, and this equation is applicable for solving both the region of solid matrix and PCM. For the region of solid matrix, the enthalpy and thermal conductivity in Eq. (1) are calculated by

$$\lambda = \lambda_{p,s} + \beta(\lambda_{p,l} - \lambda_{p,s}) \quad (2)$$

$$\lambda = \lambda_b \quad (3)$$

where λ is the thermal conductivity, subscript b represents brick or marble solid matrix, subscripts l and s represent liquid state and solid state, respectively. For the region of PCM, the phase change of solidification/melting occurs under indoor air temperature and under-floor heating flux. The enthalpy–porosity technique does not explicitly track the interface of solidification/melting but rather introduces a quantity called the liquid fraction, which was defined as

$$\left\{ \begin{array}{ll} \beta = 0 & \text{if } T > T_s \\ \beta = 1 & \text{if } T > T_l \\ \beta = (T - T_s) / (T_l - T_s) & \text{if } T_s < T < T_l \end{array} \right. \quad (4)$$

where T_s is the solidus temperature and T_l is the liquidus temperature.

Thus, the enthalpy h in the region of PCM in Eq. (1) can be calculated by

$$h = \int_0^T c_p dT + \beta L_p \quad (5)$$

where L_p is the latent heat of PCM. Thermal properties of PCM in mushy zone were assumed to be linear with temperature, so the specific heat capacity and thermal conductivity are

$$c_p = c_{p,s} + \beta(c_{p,l} - c_{p,s}) \quad (6)$$

$$\lambda = \lambda_{p,s} + \beta(\lambda_{p,l} - \lambda_{p,s}) \quad (7)$$

where subscripts p , l and s represent the PCM, liquid state and solid state, respectively.

The governing equations in indoor air region were as follows:

Energy equation

$$\frac{\partial T}{\partial \tau} + u \frac{\partial T}{\partial x} + v \frac{\partial T}{\partial y} = \frac{\lambda}{\rho_a c_{p,a}} \left(\frac{\partial^2 T}{\partial x^2} + \frac{\partial^2 T}{\partial y^2} \right) \quad (8)$$

where $c_{p,a}$ is the heat capacity and ρ_a is the density of indoor air.

Momentum equation

$$\rho_a \left(\frac{\partial \mathbf{u}}{\partial \tau} + u \frac{\partial \mathbf{u}}{\partial x} + v \frac{\partial \mathbf{u}}{\partial y} \right) = F_x - \frac{\partial P}{\partial x} + \mu \left(\frac{\partial^2 \mathbf{u}}{\partial x^2} + \frac{\partial^2 \mathbf{u}}{\partial y^2} \right) \quad (9)$$

$$\rho_a \left(\frac{\partial \mathbf{v}}{\partial \tau} + u \frac{\partial \mathbf{v}}{\partial x} + v \frac{\partial \mathbf{v}}{\partial y} \right) = F_x - \frac{\partial P}{\partial y} + \mu \left(\frac{\partial^2 \mathbf{v}}{\partial x^2} + \frac{\partial^2 \mathbf{v}}{\partial y^2} \right) \quad (10)$$

where μ is the dynamic viscosity of indoor air, F_x and F_y are body forces in x and y directions, respectively.

Continuity equation

$$\frac{\partial u}{\partial x} + \frac{\partial v}{\partial y} = 0 \quad (11)$$

3.2 Boundary conditions

For the unsteady heat transfer, the initial condition was

$$T(x, y, 0) = T_0 \quad (12)$$

T_0 is 291 K in this calculation.

Convection combined with external radiation was imposed on the left, right and top surfaces of the wall.

$$-\lambda_w \frac{\partial T}{\partial x} = h_f (T_w - T_f) + q_r \quad (13)$$

where λ_w is the thermal conductivity of wall; h_f is the heat transfer coefficient; T_w and T_f are the temperature of building envelope surface and external fluids, respectively; and q_r is the heat radiation of environment (sky, sea surface or ground).

Adiabatic wall boundary was applied to the side surface of the marble and SSPCM:

$$-\lambda \frac{\partial T}{\partial x} \Big|_{x_1, x_2} = 0 \quad (14)$$

Fixed heat flux boundary condition was applied to the bottom surface of the SSPCM layer.

$$\begin{cases} -\lambda_p \frac{\partial T}{\partial y} = C, (0 \leq \tau \leq 8\text{h}), \\ -\lambda_p \frac{\partial T}{\partial y} = 0, (8 < \tau \leq 24\text{h}), \end{cases} \quad (15)$$

where λ_p is the thermal conductivity of PCMs, and C is the under-floor heating flux.

3.3 Numerical solution

Computational fluid dynamics was used to set up a 2D heat transfer problem (Fig. 4). A grid independence test was conducted using different mesh sizes. The test proved that the results based on the final grid system presented in this work were independent of the mesh size. Solidification/melting and energy models were used to solve the problem. The heat release process was simulated through the initial condition of the temperature field after the end of heat storage, and then the heat flux was deleted.

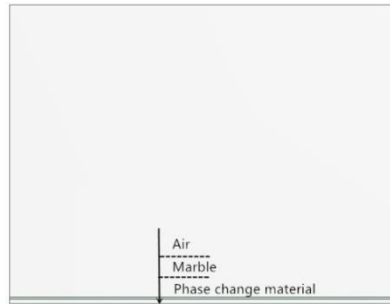


Fig. 4 Profile of room with full size on two dimensions.

Free convection and thermal radiation of the surroundings were set on the outer wall. Constant heat flux was set on the bottom of the floor. Moreover, the radiation model of surface to surface was adapted in the calculation. The mesh had two walls that formed the interface between the fluid and solid, and these interfaces were set as coupled walls.

4. Numerical results and discussion

4.1 Thermal conductivity

The heating position was set at the bottom of the SSPCM layer to obtain representative results. In the second chapter of the experimental section, the thermal conductivity of SSPCM increases from $0.35 \text{ W}/(\text{m}\cdot\text{K})$ to $1.47 \text{ W}/(\text{m}\cdot\text{K})$ upon addition of only 5% wt EG compared with that of SSPCM without EG. Furthermore, the thermal conductivity of EG reaches $300 \text{ W}/(\text{m}\cdot\text{K})$. As a result, the thermal conductivity of SSPCM increases with the addition of EG. For comparison, thermal conductivities of 0.5 , 1.5 and $4.5 \text{ W}/(\text{m}\cdot\text{K})$ were used to calculate the indoor air temperature in 24 h under the winter weather condition of Qingdao. The under-floor electric heating flux is $200 \text{ W}/\text{m}^2$. In addition, the heat fusion of SSPCM is $150 \text{ kJ}/\text{kg}$, the thickness of the SSPCM layer is 40 mm and the liquidus and solidus temperatures are $28 \text{ }^\circ\text{C}$.

Liquid fraction of PCMs with different thermal conductivities in 24 h is shown in Fig. 5, whose values are 0.7 , 0.68 and 0.67 , respectively, at the end of heat storage stage. The difference between PCM with thermal conductivity of $0.5 \text{ W}/(\text{m}\cdot\text{K})$ and the others in liquid fraction is obvious during the heat release stage.

In addition, liquid fraction of PCM with thermal conductivity of $1.5 \text{ W}/(\text{m}\cdot\text{K})$ is zero at 10:00 pm and the time advanced to 9:00 pm with thermal conductivity $4.5 \text{ W}/(\text{m}\cdot\text{K})$, whereas the liquid fraction is 0.03 with thermal conductivity of $0.5 \text{ W}/(\text{m}\cdot\text{K})$ at 12:00 pm.

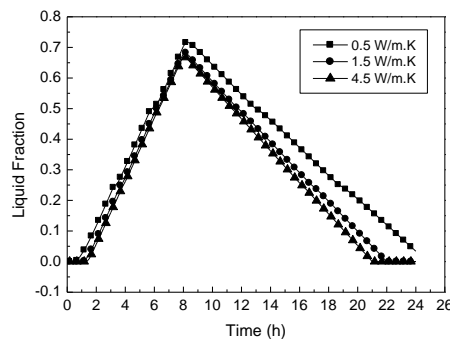


Fig. 5 Liquid fraction of PCM under different thermal conductivities.

Indoor air temperature swings with different thermal conductivities in 24 h are shown in Fig. 6. At the beginning of heat storage, indoor air temperature decreases for thermal response of floor. PCM with thermal conductivity of 0.5 W/(m·K) has lower value in indoor air temperature than the others. After 2 h heat storage, indoor air temperature increases gradually. Indoor air average temperature are 16.7 °C, 17.6 °C and 18.0 °C, respectively, when thermal conductivities of PCM are 0.5, 1.5 and 4.5 W/(m·K). Hence, the indoor air temperature increases with increasing thermal conductivity.

In addition, PCMs with high thermal conductivity exhibit small temperature fluctuation from 2 h to 22 h. However, the temperature with higher thermal conductivity falls more rapidly in the ending process because PCMs with high thermal conductivity have been completely solidified and the heat source is the sensible heat of floor, instead of the heat fusion of PCMs.

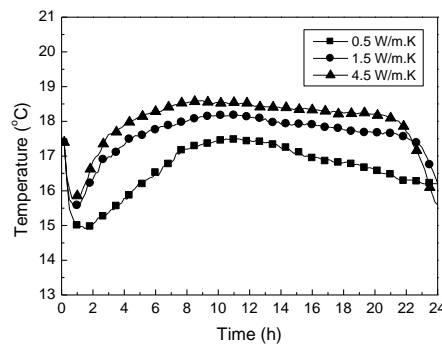


Fig. 6 Indoor air temperature swing with different thermal conductivities.

Surface temperature swings of floor with different thermal conductivities in 24 h are shown in Fig. 7. Surface temperature of floor increases for thermal response in the first 2 h. The temperature ranges from 25.8 °C to 26.2 °C, 24.9 °C to 25.8 °C and 22 °C to 24.7 °C, respectively, when thermal conductivities of PCM are 0.5, 1.5 and 4.5 W/(m·K) between 2 h and 20 h. Consequently, floor temperature increases and temperature fluctuation decreases, with increasing the thermal conductivity of PCM.

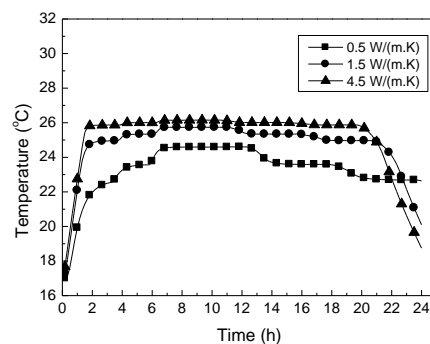


Fig. 7 Temperature swing of floor surface under different thermal conductivities.

In summary, increasing thermal conductivity increases value and decreases the fluctuation of indoor air and floor surface temperature, whereas indoor air temperature decreases rapidly with higher thermal conductivity in the ending process, and heat storage again in time is necessary.

4.2 Thickness of SSPCM layer

SSPCM layers with thicknesses of 20, 30 and 40 mm were used to calculate the indoor air temperature. Indoor air temperature swing in 24 h for different thicknesses of SSPCM layer is shown in Fig. 8.

The temperature tendency of indoor air with SSPCM layer of 20 mm shows obvious difference from the others, and the indoor air temperature shows an initial decrease, a rapid rise to 25 °C and then a rapid decrease to 18 °C.

The fluctuation of indoor air temperature are small and show a similar pattern when the thicknesses of SSPCM layer are 30 and 40 mm. The temperature is higher with 30 mm SSPCM layer than that when the thickness of SSPCM layer is 40 mm, and the difference between them is approximately 1 °C. Comfort temperature ranges from 16 °C to 20 °C for a room incorporated with floor heating system, and the temperature is from 14.5 °C to 16.5 °C when the thickness of SSPCM layer is 40 mm, which is lower than that from 15.3 °C to 17.5 °C when the thickness of SSPCM layer is 30 mm.

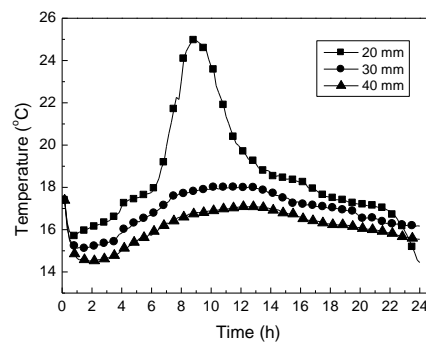


Fig. 8 Indoor air temperature swing under different SSPCM layer thicknesses

In rooms where people often stay in, the comfort floor surface temperature ranges from 24 °C to 26 °C (maximum temperature is 28 °C), and the value ranges from 28 °C to 30 °C (maximum temperature is 32 °C) for rooms where people stay in temporarily.

From 6 h to 12 h, when the thickness of SSPCM layer is 20 mm, the floor temperature is larger than 28 °C, which makes the floor surface temperature higher and makes people feel less comfort (Fig. 9). Most of the floor surface temperature ranges from 22 °C to 25 °C and 20 °C to 23 °C when the thicknesses of SSPCM layers are 30 and 40 mm, respectively. In other words, an appropriate temperature does not increase with the increment of thickness. The heat resistance increases with the increment of thickness of SSPCM layer, which slows down the heat diffusion from the floor to the indoor air.

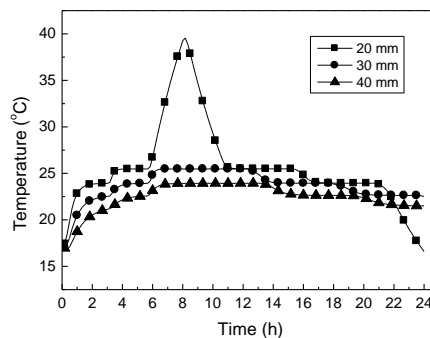


Fig. 9 Temperature swing of floor surface under different SSPCM layer thicknesses

After applying the same amount of heating time, different thicknesses of SSPCM layer produce a significant difference in the liquid fraction of the SSPCM (Fig. 10). The SSPCM layer with 20 mm thickness completely melted after 5 h and keeps a liquid status for approximately 8 h. Some solid paraffin still exists when the thicknesses are 30 and 40 mm, and the liquid fractions are 0.98 and 0.72, respectively. Consequently, increasing thickness slows the melting speed and melting degree of SSPCM.

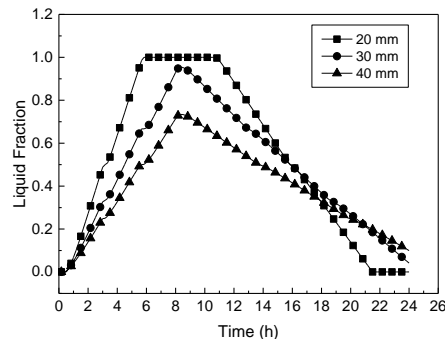


Fig. 10 Melting degree of SSPCM under different thicknesses.

4.3 Under-floor heating flux

In the study on the effect of heat flux on the thermal characteristics of the room during the heat storage and heat release stages, the thermal conductivity (λ) of PCMs is $0.35 \text{ W}/(\text{m}\cdot\text{K})$. Heat fluxes q_1, q_2 and q_3 are $150, 200$ and $250 \text{ W}/\text{m}^2$, respectively. Other physical parameters are the same as those mentioned in Section 4.1.

Liquid fractions of PCM with different heat fluxes in 24 h are shown in Fig. 11. Evidently, liquid fractions of PCMs show big difference among the three kinds of heat flux under the same conditions. The curves show similar in trends and increase gradually in heat storage period, whose liquid fractions reduce gradually as the heat is released. However, under-floor heating flux has a significant effect on the melting process of SSPCM, and the slope of the curve increases with the increase of heat flux. The maximum liquid fractions of PCM are 0.48 (8.2 h), 0.73 (8.3 h) and 0.98 (8.8 h), respectively, when the heat fluxes are $150, 200$ and $250 \text{ W}/\text{m}^2$, respectively. In other words, PCMs have not yet completely melted even if the heat flux is $250 \text{ W}/\text{m}^2$. In addition, the liquid fraction of PCMs with heat flux of $150 \text{ W}/\text{m}^2$ is zero at 20 h , and the values are 0.10 and 0.32 , respectively, when heat fluxes are 200 and $250 \text{ W}/\text{m}^2$ until the heat release is over. Consequently, latent heat as the source takes longer time in increasing heat flux with the same size of SSPCM layer.

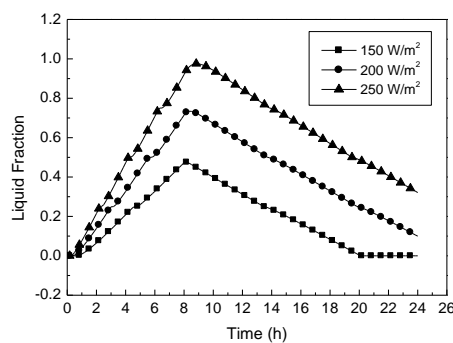


Fig. 11 Melting degree of SSPCM under different heat fluxes.

Temperature distributions of the upper and lower surfaces of the PCM during the heat storage and release stages are shown in Figs. 12 and 13. In Fig. 12, the upper surface temperature of the PCM is smaller than the melting point ($28\text{ }^{\circ}\text{C}$) of the PCM in three heat flux conditions, which obviously explains that PCM did not completely melt with a heat flux of 250 W/m^2 . In Fig. 13, the lower surface temperature of the PCM is almost constant, which indicates the advantages of small temperature fluctuation during the phase-change process.

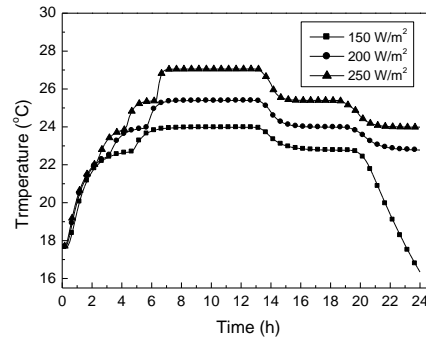


Fig. 12 Upper surface temperature of PCM layer.

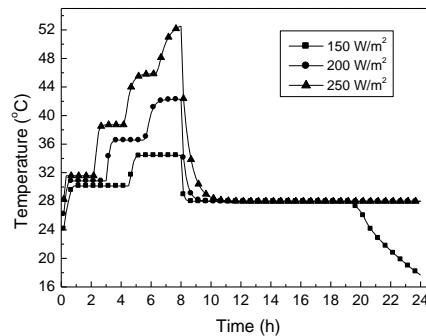


Fig. 13 Temperature of lower-surface PCM layer.

Indoor air temperature swings during the heat storage and heat release stages are shown in Fig. 14. The tendencies of the three curves are similar. When heat storage has been approximately 2 h, the room temperature began to rise. Indoor air temperature was kept stable during 9 h to 13 h and gradually decreased as time goes on. However, a rapidly fall begins at 21 h when the heat fusion is 150 W/m^2 because PCM completely solidified at 20 h and sensible heat (smaller in quantity than latent heat) is the only source to floor during this time.

When heat fluxes are 150 , 200 and 250 W/m^2 , indoor air temperature over $16\text{ }^{\circ}\text{C}$ ranges from 9 h to 15 h, 6.5 h to 20.5 h and 5.1 h to 24 h, respectively; indoor air average temperatures are $15.4\text{ }^{\circ}\text{C}$, $16.1\text{ }^{\circ}\text{C}$ and $16.8\text{ }^{\circ}\text{C}$, respectively; and indoor air maximum temperatures are $16.8\text{ }^{\circ}\text{C}$, $17.0\text{ }^{\circ}\text{C}$ and $18.0\text{ }^{\circ}\text{C}$, respectively. To conclude, indoor air temperature increases with increasing heat flux, and heat flux has a significant influence on the thermal performance of room with SSPCM.

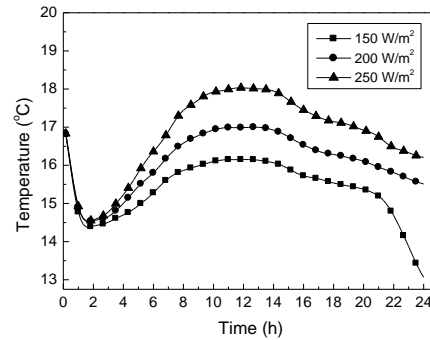


Fig. 14 Temperature of room under different heat fluxes.

4.4 Heat fusion

Heat fusions of 150, 200 and 250 kJ/kg were used to calculate the thermal performance of room. Liquid fractions of PCMs with different heat fusions in 24 h are shown in Fig. 15. The tendencies of indoor air temperature show a similar pattern but different amplitude. Liquid fractions are 0.71, 0.54 and 0.47 when heat fusions are 150, 200 and 250 kJ/kg, respectively, at the end of heat storage stage, and these data indicate that liquid fraction decreases with increasing heat fusion. Liquid fractions are 0.1, 0.09 and 0.09 at the end of heat release stage. In other words, all PCMs retain some liquid phase until heat release stage is over.

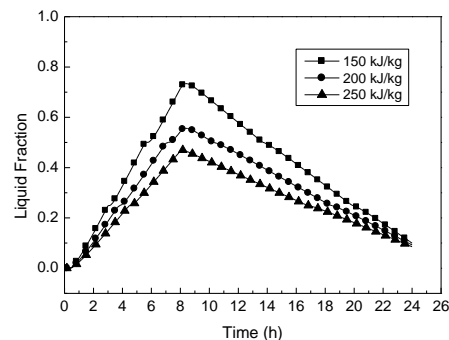


Fig. 15 Melting degree of SSPCM under different heat fusions.

Indoor air temperature swings with different thermal conductivities in 24 h are shown in Fig. 16. The heat fusion of 250 kJ/kg has smaller temperature fluctuation than the others, and the maximum indoor air temperature increases with decreasing heat fusion.

When heat fusions are 150, 200 and 250 kJ/kg, the indoor average temperatures are 16.1 °C, 15.8 °C and 15.6 °C, and the maximum indoor temperatures are 17.1 °C, 16.9 °C and 16.3 °C, respectively. As mentioned before, for the floor radiant heating room, the comfort temperature ranges from 16 °C to 20 °C, and the durations of indoor air temperature over 16 °C are between 6.5 h and 20 h, 7.5 h and 18.5 h and 8.3 h and 16.7 h when heat fusion values are 150, 200 and 250 kJ/kg, respectively. Apparently, increasing heat fusion lowers indoor air temperature and extends the time of comfort temperature, because the amount of heat absorbed by PCMs increases with the increasing heat fusion. As a result, the amount of heat transferred to room is decreased, which reduces indoor air average temperature.

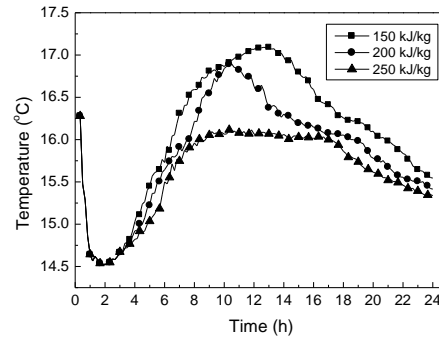


Fig. 16 Indoor air temperature swing under different SSPCM heat fusions.

Surface temperature swings of floor with different heat fusions in 24 h are shown in Fig. 17. The temperature has a small range from 21.5 °C to 22.6 °C, and the average temperature is 22.2 °C when heat fusion is 250 kJ/kg between 2 h and 20 h. Fluctuation is obvious when heat fusion is 200 kJ/kg, and the value ranges from 21.5 °C to 24 °C with an average temperature of 22.6 °C. When heat fusion is 200 kJ/kg, floor surface temperature ranges from 21.5 °C to 24.0 °C and the average value is 23 °C. Consequently, although floor surface temperature decreases slightly with increasing heat fusion, the fluctuation is smaller.

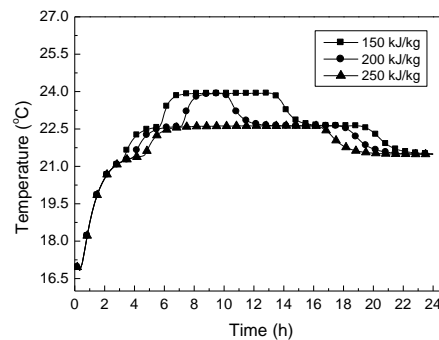


Fig. 17 Temperature of floor surface under different SSPCM latent heat values.

4.5 Temperature distribution of indoor air

To value the comfort of indoor air temperature, the significant evaluation index is the uniformity of temperature distribution in horizontal and vertical directions.

A peak value in each temperature curve is seen, which is approximately 2 °C higher than the average value. The reason behind this finding is that a symmetrical vortex appears in the room cross section, which forms a symmetrical temperature and velocity distribution, as shown in Fig. 18. As a result, temperature superposition increases the intermediate temperature.

At the beginning of heat storage (before 4 h), the temperature difference is approximately 0.6 °C, and the value stays within 0.1, whereas the temperature difference is approximately 0.4 °C at the end of the process. In summary, the fluctuation is small in the horizontal direction. Hence, the uniformity of temperature distribution in horizontal is large.

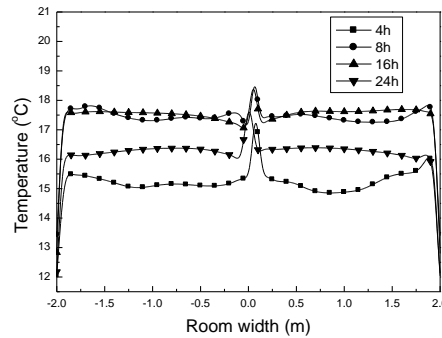


Fig. 18 Temperature distribution in horizontal direction at different times.

The distributions of indoor air temperature in vertical direction are shown in Fig. 19. To conclude, the temperature distribution is uniform in space (ranges from 100 mm to 2000 mm) where people often stay. In the 24-h duration, from the floor to the ceiling in the vertical direction, the indoor air temperature gradually decreased, and the temperature gradient is -0.4 K/m. As a result, the area near the floor surface is warm and the area near the ceiling is less warm, which is in accordance with the theory of traditional Chinese medicine, which states, ‘it is healthy to keep your foot warmer than your head’, and with the human body comfort in conformity with the law. Therefore, the process easily meets the requirements of comfort.

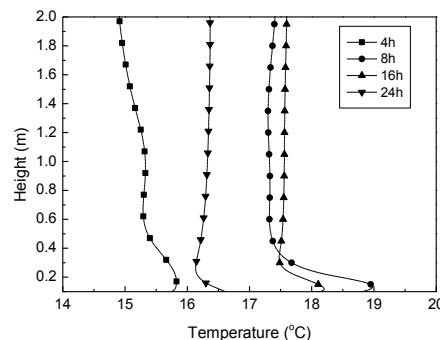


Fig. 19 Indoor air temperature distribution in vertical direction for different times.

5. Conclusions

A good knowledge on the dynamic energy performance of buildings incorporating thermal heat storage systems with PCM is essential for building researchers and practitioners to understand the building temperature response characteristics and the economic feasibility of using PCM. In this work, a full-size two-dimensional heat transfer model is abstracted from a kind of under-floor electric heating system with SSPCM floor. Aside from the calculation of heat transfer in the phase change from solid to liquid, a variety of heat transfer mechanism of the coupled problems were also considered in this model, and the thermal performance of a room with SSPCM was analyzed under different factors including thermal conductivity, thickness of SSPCM layer and under-floor heating flux.

To conclude, the thermal conductivity has obvious influence on indoor air temperature, and the higher the thermal conductivity, the better the heat diffusion. Moreover, an appropriate temperature does not increase with the increment of thickness, and the heat resistant is bigger when the thickness of SSPCM layer increases, which has a negative effect on the heat transfer from the floor to the indoor air. In addition, the heat storage time must be controlled in case the

floor temperature is too high when the SSPCM layer is less than 20 mm. More importantly, the larger the under-floor heating flux, the higher the indoor air temperature. However, the investment and comfort should balance.

Acknowledgements

This research was supported by the Residential Housing Project in Shandong and the Urban-rural Development Science and Technology Program with Grant No. 2014KY047.

References

- [1] P. Moreno, C. Solé, A. Castell, L. F. Cabeza, *Renewable & Sustainable Energy Reviews*, **39**(6), 1 (2014).
- [2] X. Sun, Q. Zhang, M. A. Medina, S. Liao, *Applied Energy* **147**, 325-334 (2015).
- [3] F. Agyenim, N. Hewitt, P. Eames, M. Smyth, *Renewable & Sustainable Energy Reviews*, **14**(2), 615 (2010).
- [4] H. Ye, X. S. Ge, *Solar Energy Materials & Solar Cells*, **64**(1), 37 (2000).
- [5] M. Xiao, B. Feng, K. Gong, *Energy Conversion & Management*, **43**(1), 103 (2002).
- [6] P. Qin, Y. Rui, Y. Zhang, K. Lin, *Journal of Tsinghua University*, **43**(6), 833 (2003).
- [7] Z. Zhang, N. Zhang, J., Peng, X. Fang, X. Gao, Y. Fang, *Applied Energy* **91**(1), 426 (2012).
- [8] W. Cheng, B. Xie, R. Zhang, Z. Xu, Y. Xia, *Applied Energy*, **144**, 10 (2015).
- [9] R. Siegel, *International Journal of Heat & Mass Transfer*, **20**(10), 1087 (1977).
- [10] H. Zou, S. Wu, J. Shen, *Chemical Reviews*, **108**(9), 3893-957 (2008).
- [11] B. Zalba, José Ma Marín, L. F. Cabeza, H. Mehling, *Applied Thermal Engineering*, **23**(3), 251 (2003).
- [12] D. B. Crawley, L. K. Lawrie, F. C. Winkelmann, W. F. Buhl, Y. J., Huang, C. O. Pedersen, et al., *Energy & Buildings*, **33**(4), 319 (2001).
- [13] A. Tardieu, S. Behzadi, J. J. J. Chen, M. M. Farid, Computer simulation and experimental measurements for an experimental pcm-impregnated office building., *Proc Building Simulation* (2011).
- [14] P. C. Tabares-Velasco, C. Christensen, M. Bianchi, *Building & Environment*, **54**(7), 186 (2012).
- [15] N. Zhu, Liu, P., Hu, P., Liu, F., & Jiang, Z. *Energy & Buildings*, **107**, 181-190 (2015).
- [16] X. Xu, Y. Zhang, K. Lin, H. Di, R. Yang, *Energy & Buildings*, **37**(10), 1084-1091 (2005).
- [17] Y. Dutil, D. R. Rousse, N. B. Salah, S. Lassue, L. Zalewski, *Renewable & Sustainable Energy Reviews* **15**(1), 112-130 (2011).
- [18] V. R. Voller, C. Prakash, *International Journal of Heat & Mass Transfer* **30**(8), 1709 (1987).
- [19] V. R. Voller, & C. R. Swaminathan., *Numerical Heat Transfer Fundamentals* **19**(2), 175 (1991).
- [20] V. R. Voller. *Numerical Heat Transfer Fundamentals*, **17**(2), 155 (1990).
- [21] C. R. Swaminathan, V. R. Voller, *Metallurgical and Materials Transactions B*, **23**(5), 651 (1992).